Controlled Injection of Spin-Triplet Supercurrents into a Strong Ferromagnet

J. W. A. Robinson, *et al.*

Science **329**, 59 (2010);
DOI: 10.1126/science.1189246

3. F. Crifo, A. Vidal-Madjar, R. Lallement, R. Ferlet, M. Gerbaldi, *Astron. Astrophys.* **320**, L29 (1997).
4. B. A. Smith, R. J. Terrile, *Science* **226**, 1421 (1984).
5. A. M. Lagrange, D. E. Backman, P. Artymowicz, in *Protostars and Planets IV*, V. Mannings, A. P. Boss, S. S. Russel, Eds. (Univ. of Arizona Press, Tuscon, AZ, 2000), pp. 639–672.
6. M. Wyatt, *Annu. Rev. Astron. Astrophys.* **46**, 339 (2008).
7. C. M. Telesco *et al.*, *Nature* **433**, 133 (2005).
8. Z. Wahhaj *et al.*, *Astrophys. J.* **584**, L27 (2003).
9. Y. K. Okamoto *et al.*, *Nature* **431**, 660 (2004).
10. P. Kalas, D. Jewitt, *Astron. J.* **110**, 794 (1995).
11. D. A. Golimowski *et al.*, *Astron. J.* **131**, 3109 (2006).
12. S. R. Heap *et al.*, *Astrophys. J.* **539**, 435 (2000).
13. D. Mouillet, J. D. Larwood, J. C. B. Papaloizou, A. M. Lagrange, *Mon. Not. R. Astron. Soc.* **292**, 896 (1997).
14. J. C. Augereau, R. P. Nelson, A. M. Lagrange, J. C. B. Papaloizou, D. Mouillet, *Astron. Astrophys.* **370**, 447 (2001).
15. A. Vidal-Madjar, A. Lecavelier, R. Ferlet, *Planet. Space Sci.* **46**, 629 (1998).
16. I. Pascucci, S. Tachibana, in *Protoplanetary Dust*, D. Apai, D. Lauretta, Eds. (Cambridge Univ. Press, Cambridge, 2010), pp. 263–298.
17. H. Beust, A. Morbidelli, *Icarus* **143**, 170 (2000), and references therein.
18. A. M. Lagrange *et al.*, *Astron. Astrophys.* **493**, L21 (2009).
19. A. M. Lagrange *et al.*, *Astron. Astrophys.* **506**, 927 (2009).
20. M. P. Fitzgerald, P. G. Kalas, J. R. Graham, *Astrophys. J.* **706**, L41 (2009).
21. G. Rousset *et al.*, *Proc. SPIE* **4839**, 140 (2003).
22. R. Lenzen *et al.*, *Proc. SPIE* **4841**, 944 (2003).
23. I. Baraffe, G. Chabrier, T. S. Barman, F. Allard, P. H. Hauschildt, *Astron. Astrophys.* **402**, 701 (2003).
24. J. J. Fortney, M. S. Marley, D. Saumon, K. Lodders, *Astrophys. J.* **683**, 1104 (2008).
25. G. Olofsson, R. Liseau, A. Brandeker, *Astrophys. J.* **563**, L77 (2001).
26. F. Freistetter, A. V. Krivov, T. Löhne, *Astron. Astrophys.* **466**, 389 (2007).
27. A. Lecavelier des Etangs, A. Vidal-Madjar, *Astron. Astrophys.* **497**, 557 (2009).
28. C. Marois *et al.*, *Science* **322**, 1348 (2008); published online 13 November 2008 (10.1126/science.1166585).
29. P. Kalas *et al.*, *Science* **322**, 1345 (2008); published online 13 November 2008 (10.1126/science.1166609).
30. P. Kalas, J. R. Graham, M. Clampin, *Nature* **435**, 1067 (2005).
31. K. Y. L. Su *et al.*, *Astrophys. J.* **705**, 314 (2009).
32. The 3- to 7-M_{Jup} companion to the brown dwarf 2Mass1207 also formed in less than 5 to 12 My. However, its formation process (stellarlike or through gravitational instability within disk) is still a matter of debate.
33. G. M. Kennedy, S. J. Kenyon, *Astrophys. J.* **673**, 502 (2008).
34. S. Ida, D. N. C. Lin, *Astrophys. J.* **685**, 584 (2008).

35. We thank ESO staff, especially C. Melo, C. Dumas, and J. Girard for their help. We acknowledge financial support from the Programme National de Planétologie Institut National des Sciences de l'Univers, as well as from the Agence Nationale pour la Recherche (grant NT05-4_4463). D.E. acknowledges support from the Centre National d'Etudes Spatiales. We also thank H. Beust, P. Rubini, and D. Collardey.

Supporting Online Material

www.sciencemag.org/cgi/content/full/science.1187187/DC1
SOM Text
Figs. S1 to S4
Tables S1 and S2
References and Notes

18 January 2010; accepted 1 June 2010
Published online 10 June 2010;
10.1126/science.1187187
Include this information when citing this paper.

Controlled Injection of Spin-Triplet Supercurrents into a Strong Ferromagnet

J. W. A. Robinson,* J. D. S. Witt, M. G. Blamire

The superconductor-ferromagnet proximity effect describes the fast decay of a spin-singlet supercurrent originating from the superconductor upon entering the neighboring ferromagnet. After placing a conical magnet (holmium) at the interface between the two, we detected a long-ranged supercurrent in the ferromagnetic layer. The long-range effect required particular thicknesses of the spiral magnetically ordered holmium, consistent with spin-triplet proximity theory. This enabled control of the electron pairing symmetry by tuning the degree of magnetic inhomogeneity through the thicknesses of the holmium injectors.

The electronic properties of a material that has been cooled below its superconducting transition temperature are influenced by the pairing symmetry of the electrons. In a conventional superconductor, the Cooper pairs are formed from electrons with an antiparallel spin alignment and are in the spin-singlet state (*1*, *2*). In contrast to superconductivity, ferromagnetism favors a parallel alignment of electron spins. Consequently, superconductivity and ferromagnetism rarely coexist, and diverse and complex phenomena arise at the interface between superconducting and ferromagnetic thin films (*3*). The most striking manifestation happens when spin-singlet Cooper pairs pass through a ferromagnet: The differential action of the ferromagnetic exchange field creates a spatially varying phase, which results in an oscillatory damping of the critical current (I_C) over a ferromagnetic thickness of a few nanometers (*4*–*10*).

Recent experiments have detected a longer-ranged effect in which the superconductivity appears to be insensitive to ferromagnetic exchange fields (*11*, *12*). These results could be explained in the context of spin-triplet pairing in which Cooper pairs are formed with a parallel spin alignment at the superconductor-ferromagnet interface (*13*–*15*). The spin-triplet pair is believed to be only weakly affected by the exchange field so that its phase coherence decays on the same length scale as that of spin-singlet pairs in a normal metal. Within this theoretical framework, the generation of spin-triplet electron pairs requires the presence of particular magnetic inhomogeneity at the superconductor-ferromagnet interface (*13*, *16*).

Long-range Josephson coupling is presently the most robust way of detecting a spin-triplet current, and was reported in (*11*, *12*) for a barrier formed from the half-metal CrO_2. Supporting theory (*14*) suggested that the required magnetic inhomogeneity for the spin-triplet proximity effect could be provided by hypothetical spin disorder at the surface of the half-metal. A more recent theory (*16*) indicates that two matched spin-triplet sources are needed to achieve a Josephson effect; physically, this condition requires both interfaces to be magnetically noncollinear and to share specific symmetries. Because the nature of the inhomogeneteity is uncertain in the CrO_2-based junctions, reproducibly achieving these symmetry requirements in

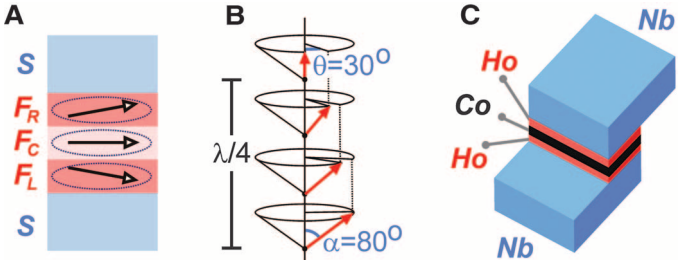

Fig. 1. (**A**) Theoretical spin-triplet Josephson junction adapted from (*16*), consisting of two spin-singlet superconductors (*S*) linked via a noncollinear ferromagnetic trilayer (F_L-F_C-F_R). (**B**) The conical magnetic configuration of idealized Ho below its Curie temperature (20 K), showing an antiferromagnetic spiral rotating in-plane by θ = 30° per atomic plane and pitched α = 80° out-of-plane. The moments (arrows) rotate about the surface of a cone with the spiral wavelength, λ, corresponding to a Ho thickness of ~3.4 nm. (**C**) Device layout consisting of two superconducting Nb electrodes coupled via a Ho-Co-Ho trilayer.

Department of Materials Science and Metallurgy, University of Cambridge, Pembroke Street, Cambridge CB2 3QZ, UK.

*To whom correspondence should be addressed. E-mail: jjr33@cam.ac.uk

this system is challenging. An enhanced proximity effect was also recently reported in (*17*); here the likely source of magnetic inhomogeneity was in secondary ferromagnet/normal metal bilayers placed at the superconductor/ferromagnet interface.

For a more straightforward interpretation of the results, an appealing approach would be to use one of the intrinsically inhomogeneous ferromagnets such as the rare earth metal Ho (*18*) coupled to a homogeneous ferromagnetic barrier. Long-range superconducting phase-coherent oscillations were reported in Ho wires (*19*) grown by evaporation and contacted inside a superconducting ring, but a Josephson current was not detected.

Our experiment was motivated by the proposal (*16*) for a spin-triplet Josephson junction consisting of two spin-singlet superconductors (S) coupled via a ferromagnetic trilayer ($F_L/F_C/F_R$). The magnetization of F_L and F_R layers should be noncollinear to provide the necessary inhomogeneity for the spin-triplet configuration of electron spins to be favorable (Fig. 1A). The experiment enables the decay length of the supercurrent from spin-triplet pairs in the homogeneous central ferromagnet F_C to be directly compared with that in simple homogeneous ferromagnetic barriers of the same material and thickness.

We report results from structures in which Ho was used for F_L and F_R, and Co was used for F_C (Fig. 1, B and C). The conical magnetic ordering of Ho, which consists of an antiferromagnetic spiral canted to produce a net ferromagnetic component in the *c*-axis orientation, allows for the inclusion of reproducibly noncollinear magnetic layers within device structures. Moreover, its magnetic properties and a preferential (0001) texture are robust even in thin films at the nanometer scale (*20*).

We processed several series of nanoscale Nb/Ho/Co/Ho/Nb junctions with varying Ho and Co layer thicknesses (*21*); within each junction, the thicknesses of F_L and F_R Ho layers were equal and varied in the 0- to 12-nm range with an absolute error of ~0.2 nm. The electrical properties of these junctions were measured at 4.2 K, from which the critical current (I_C) and normal state resistance (R_N) of a device were determined (*21*). Because device areas varied, I_C was normalized by multiplying by R_N to give the characteristic voltage (I_CR_N).

The behavior of simple Co barrier junctions is well understood: The singlet-based I_C oscillates as a function of Co thickness with a period of ~1 nm superimposed on an exponentially decaying function with a characteristic length of ξ_{Co} ~1 nm [Fig. 2A, inset; data from Nb/Rh/Co/Rh/Nb junctions in (*22*)]. This structure was chosen because it represents an equivalent layering sequence with the same number of interfaces and therefore acts as a better control sample than a pure Nb/Co/Nb junction (which nevertheless shows similar properties).

The main plot in Fig. 2A shows the Co thickness dependence of I_CR_N for Nb/Ho/Co/Ho/Nb junctions. In comparison with the Co barrier junctions, the decay length is substantially longer by a factor of at least 20. The figure shows an approximate fit (shaded region) giving a coherence length of $\xi_{Co} > 10$ nm, which agrees with the normal (nonmagnetic) coherence length $(\hbar D/k_BT)^{1/2} \sim 10$ nm assuming an electron diffusivity of $D \approx 4.3 \times 10^{-7}$ m^2 s^{-1} (and where $\hbar$ is Planck's constant h divided by 2π, k_B is Boltzmann's constant, and T is temperature) (*22*); that is, the supercurrent is passing through the composite Ho/Co/Ho barrier as if it were nonmagnetic.

To understand in more detail the role of the Ho layers, we symmetrically varied d_{Ho} [any asymmetry (Δd_{Ho}) < 0.2 nm]) for several values of Co barrier thicknesses (Fig. 2B). In the 2-nm Co data, increasing the thickness of the Ho layers results in an increase in I_CR_N of more than an order of magnitude, despite the overall increase in barrier thickness and total magnetic moment. Plain Co barriers of 5 and 8 nm show no measurable supercurrent in our previous experiments (*9*, *22*). Further measurements confirming the presence of a Josephson effect are given in Fig. 3, A and B. External microwaves give rise to sharp dips in the dynamic resistance at particular voltage (V) values (Fig. 3A). These Shapiro steps occur at integer values of $V/\varphi_0 f = \pm 1$, where φ_0 is the flux quantum and f is the applied microwave frequency. Upon application

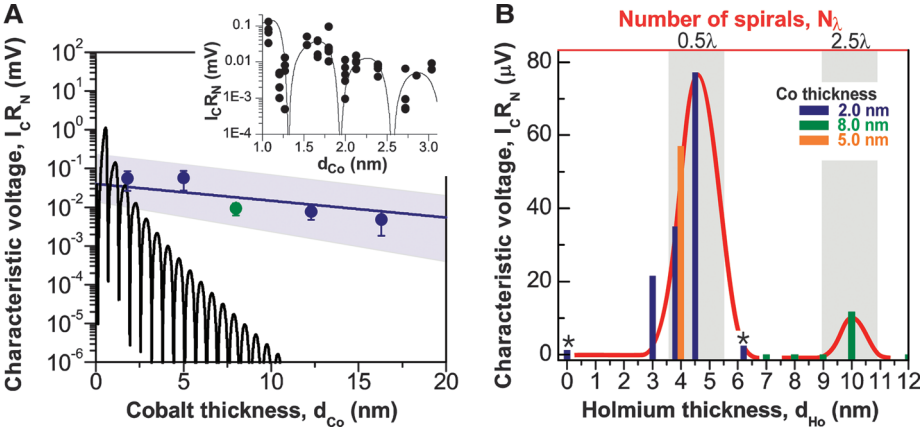

Fig. 2. (**A**) Slow decay at 4.2 K in the characteristic voltage of Nb/Ho(4.5 nm)/Co(d_{Co})/Ho(4.5 nm)/Nb junctions (blue circles) and Nb/Ho(10 nm)/Co(d_{Co})/Ho(10 nm)/Nb junctions (green circles) versus Co barrier thickness (d_{Co}). Inset: Comparative data (black circles) from (*22*) showing the behavior of Nb/Rh/Co/Rh/Nb junctions. The oscillating curves in the inset and main panel are theoretical fits to the experimental data in the inset, as described in (*22*). (**B**) Characteristic voltage in Nb/Ho(d_{Ho})/Co/Ho(d_{Ho})/Nb junctions at 4.2 K versus Ho layer thickness (d_{Ho}) for various Co barrier thicknesses. The thicknesses of each Ho layer in a junction are identical. The peaks correlate to noninteger spiral wavelengths (λ) in Ho. Asterisks identify small, but nonzero characteristic voltage values. The red curves are a guide to the eye.

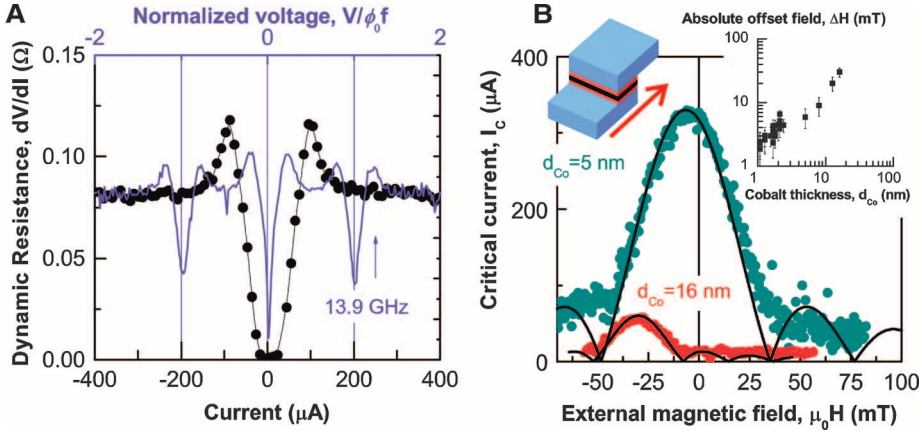

Fig. 3. (**A**) Dynamic resistance of a Nb/Ho(4.5 nm)/Co(16 nm)/Ho(4.5 nm)/Nb junction versus current and voltage at 4.2 K with and without microwaves. The normal state resistance of this device is $R_N \approx 0.076$ ohm and the critical current is $I_C \approx 90$ μA. The voltage scale is divided by $\varphi_0 f$, where φ_0 is the flux quantum and f is the microwave frequency. A constant in-plane field of −32 mT was applied during these measurements to cancel out internal flux and demagnetizing fields from the Co barrier. (**B**) Critical current versus in-plane magnetic field at 4.2 K. The critical currents are offset in field (ΔH) due to internal flux and demagnetizing fields from the Co barrier. Solid curves are a guide to the eye. Insets: (left) illustration of a junction showing the field orientation, and (right) absolute ΔH versus Co barrier thickness.

of an external in-plane magnetic field (H) to our junctions, we observe a Fraunhofer-like dependence of I_C on H. The maximum I_C values are, however, offset from zero field (ΔH) due to the presence of internal flux and demagnetizing fields from the Co barriers. The absolute value of ΔH linearly depends on the Co barrier thickness (Fig. 3B inset), demonstrating that the Co barriers are monodomain in nature (*21*).

Taken together, the data in Fig. 2, A and B, show a complex variation of $I_C R_N$ over the thickness range investigated, with peaks corresponding to Ho thicknesses of ~4.5 and ~10 nm. By measuring the saturation magnetization of a series of Nb/Ho/Co/Ho/Nb control samples, we determined a magnetically "dead" layer of ~1.2 nm per Ho surface (*21*) (fig. S1A). Thus, the peaks in $I_C R_N$ in Fig. 2B correspond to magnetic Ho layer thicknesses of ~2.2 and ~7.8 nm, which are comparable to the experimentally determined coherence length in Ho of $\xi_{Ho} \sim 5$ nm (*21*). This is then broadly consistent with the analysis in (*16*), in which the largest spin-triplet contribution to I_C is predicted to occur when F_L and F_R layers have a thickness in the (0.5 to 2.5)ξ range. However, this cannot on its own explain the peak structure, and so we considered a possible link between the peak thicknesses and the known spiral wavelength of Ho, $\lambda \sim 3.4$ nm (*23*). Factoring in the magnetically dead layer of Ho implies that the peak values of $I_C R_N$ correspond to antiferromagnetic spiral wavelengths of ~λ/2 and ~5(λ/2). Although an exact parallel between these peaks and the magnetic ordering cannot be drawn from this analysis, it is nevertheless clear that the peaks appear at thicknesses corresponding to a high level of inhomogeneity in the Ho, i.e., at thicknesses in which the spirals are incomplete.

The long-range effect reported cannot be explained in terms of a spin-singlet proximity theory or a complex domain-wall–related phenomenon (*24*, *25*). A controllable supercurrent with a finite spin projection can allow for a more complete interaction between superconductivity and magnetism, possibly bringing together the previously disparate fields of superconductivity and spin-electronics (*26*, *27*).

References and Notes

1. J. Bardeen, L. N. Cooper, J. R. Schrieffer, *Phys. Rev.* **106**, 162 (1957).
2. J. Bardeen, L. N. Cooper, J. R. Schrieffer, *Phys. Rev.* **108**, 1175 (1957).
3. A. I. Buzdin, *Rev. Mod. Phys.* **77**, 935 (2005).
4. T. Kontos, M. Aprili, J. Lesueur, X. Grison, *Phys. Rev. Lett.* **86**, 304 (2001).
5. V. V. Ryazanov *et al.*, *Phys. Rev. Lett.* **86**, 2427 (2001).
6. Y. Blum, A. Tsukernik, M. Karpovski, A. Palevski, *Phys. Rev. Lett.* **89**, 187004 (2002).
7. C. Bell, R. Loloee, G. Burnell, M. G. Blamire, *Phys. Rev. B* **71**, 180501(R) (2005).
8. F. Born *et al.*, *Phys. Rev. B* **74**, 140501(R) (2006).
9. J. W. A. Robinson, S. Piano, G. Burnell, C. Bell, M. G. Blamire, *Phys. Rev. Lett.* **97**, 177003 (2006).
10. A. A. Bannykh *et al.*, *Phys. Rev. B* **79**, 054501 (2009).
11. R. S. Keizer *et al.*, *Nature* **439**, 825 (2006).
12. M. S. Anwar, M. Hesselberth, M. Porcue, J. Aarts, http://arxiv.org/abs/1003.4446 (2010).
13. F. S. Bergeret, A. F. Volkov, K. B. Efetov, *Rev. Mod. Phys.* **77**, 1321 (2005).
14. M. Eschrig, T. Löfwander, *Nat. Phys.* **4**, 138 (2008).
15. J. Linder, T. Yokoyama, A. Sudbø, M. Eschrig, *Phys. Rev. Lett.* **102**, 107008 (2009).
16. M. Houzet, A. I. Buzdin, *Phys. Rev. B* **76**, 060504(R) (2007).
17. T. S. Khaire, M. A. Khasawneh, W. P. Pratt Jr., N. O. Birge, *Phys. Rev. Lett.* **104**, 137002 (2010).
18. S. Chikazumi, *Physics of Ferromagnetism* (Clarendon, Oxford, 1997).
19. I. Sosnin, H. Cho, V. T. Petrashov, A. F. Volkov, *Phys. Rev. Lett.* **96**, 157002 (2006).
20. C. Schussler-Langeheine *et al.*, *J. Electron Spectrosc. Relat. Phenom.* **114–116**, 953 (2001).
21. Materials and methods are available as supporting material on *Science* Online.
22. J. W. A. Robinson, Z. H. Barber, M. G. Blamire, *Appl. Phys. Lett.* **95**, 192509 (2009).
23. W. C. Koehler, J. W. Cable, M. K. Wilkinson, E. O. Wollan, *Phys. Rev.* **151**, 414 (1966).
24. A. F. Volkov, K. B. Efetov, *Phys. Rev. B* **78**, 024519 (2008).
25. Ya. V. Fominov, A. F. Volkov, K. B. Efetov, *Phys. Rev. B* **75**, 104509 (2007).
26. T. Löfwander, T. Champel, J. Durst, M. Eschrig, *Phys. Rev. Lett.* **95**, 187003 (2005).
27. V. Braude, Y. M. Blanter, *Phys. Rev. Lett.* **100**, 207001 (2008).

28. J.W.A.R. acknowledges support from St. John's College, Cambridge, through a Research Fellowship. We thank G. Hálász for valuable discussions. This work was funded by the UK Engineering and Physical Sciences Research Council (EP/E026206;EP/E026532/1;EP/D001536/1).

Supporting Online Material

www.sciencemag.org/cgi/content/full/science.1189246/DC1
Materials and Methods
Fig. S1
References

8 March 2010; accepted 24 May 2010
Published online 10 June 2010;
10.1126/science.1189246
Include this information when citing this paper.

Quantized Anomalous Hall Effect in Magnetic Topological Insulators

Rui Yu,[1] Wei Zhang,[1] Hai-Jun Zhang,[1,2] Shou-Cheng Zhang,[2,3] Xi Dai,[1]* Zhong Fang[1]*

The anomalous Hall effect is a fundamental transport process in solids arising from the spin-orbit coupling. In a quantum anomalous Hall insulator, spontaneous magnetic moments and spin-orbit coupling combine to give rise to a topologically nontrivial electronic structure, leading to the quantized Hall effect without an external magnetic field. Based on first-principles calculations, we predict that the tetradymite semiconductors Bi_2Te_3, Bi_2Se_3, and Sb_2Te_3 form magnetically ordered insulators when doped with transition metal elements (Cr or Fe), in contrast to conventional dilute magnetic semiconductors where free carriers are necessary to mediate the magnetic coupling. In two-dimensional thin films, this magnetic order gives rise to a topological electronic structure characterized by a finite Chern number, with the Hall conductance quantized in units of e^2/h (where e is the charge of an electron and h is Planck's constant).

The anomalous Hall effect (AHE) (*1*, *2*), in which a voltage transverse to the electric current appears even in the absence of an external magnetic field, was first detected in ferromagnetic (FM) metals in 1881 and later found to arise from the spin-orbit coupling (SOC) between the current and magnetic moments. Recent progress on the mechanism of AHE has established a link between the AHE and the topological nature of the Hall current by adopting the Berry-phase concepts (*3*–*5*) in close analogy to the intrinsic spin Hall effect (*6*, *7*). Given the experimental discovery of the quantum Hall (*8*) and the quantum spin Hall (QSH) effects (*9*, *10*), it is natural to ask whether the AHE can also be quantized.

A simple mechanism for a quantum anomalous Hall (QAH) insulator has been proposed in a two-band model of a two-dimensional (2D) magnetic insulator (*11*). In the limit of vanishing SOC and large enough exchange splitting, the majority spin band is completely filled and the minority spin band is empty. When the exchange splitting is reduced, the two bands intersect each other, leading to a band inversion. The degeneracy at the interaction region can be removed by turning on the SOC, giving rise to an insulator state with a topologically nontrivial band structure characterized by a finite Chern number and chiral edge states characteristic of the QAH state (*11*). Alternative mechanisms of realizing the QAH state include bond currents on a honeycomb lattice (*12*) and the localization of the band electrons (*13*). However, these mechanisms may be harder to realize experimentally.

The crucial criteria for realizing a QAH state are (i) a FM 2D insulator that breaks the time-reversal symmetry and (ii) a band inversion transition with strong SOC. QSH insulators are a good starting point for the search for the QAH effect because they satisfy the second criterion.

[1]Beijing National Laboratory for Condensed Matter Physics, and Institute of Physics, Chinese Academy of Sciences, Beijing 100190, China. [2]Department of Physics, McCullough Building, Stanford University, Stanford, CA 94305–4045, USA. [3]Center for Advanced Study, Tsinghua University, Beijing 100084, China.

*To whom correspondence should be addressed. E-mail: daix@aphy.iphy.ac.cn (X.D.); zfang@aphy.iphy.ac.cn (Z.F.)